Supplementary Materials

Table of Contents

Detailed methods

Single cell RNA sequencing

Preparation of single-cell suspension. Mouse kidneys were perfused with 2ml DPBS to remove circulating PBMCs and RBCs. Then kidneys were weighed and transferred into GentleMACSTM-C tubes (Miltenyi Biotec Inc., CA) containing 6ml DPBS, 200µl Enzyme-D, 100µl Enzyme-R, and 25µl Enzyme A and DNAse (Multi Tissue Dissociation Kit-1, Miltenyi Biotec) and then run on a GentleMACS Octo dissociator (Miltenyi Biotec) for about 20 minutes. Digestion was stopped by adding MACS buffer with 1% FBS. Cells were then filtered by passing through a 100µm cell strainer, then were centrifuged at 200G for 10 minutes. The supernatant was discarded, and cells made into a single cell suspension and flow-sorted on BD Aria-III to remove RBCs, debris, and dead cells (Fig. 2A).

Single-cell RNA sequencing using 10x Genomics platform. Flow sorted cells were counted and their viability measured using a Vi-Cell XR Cell Viability Analyzer (Beckman-Coulter). The viability of all the samples was >90%. The Barcoded Gel Beads were thawed from -80Cº and the cDNA master mix prepared according to the manufacturer's instructions for the Chromium Single Cell 3' library kit, version 2 (10x Genomics).

RNA sequencing and generation of data matrix.

Libraries were sequenced at an average coverage of 15,000 reads/cell following Illumina's standard protocol using the Illumina cBot and Paired-end cluster kit version 3. The flow cells were sequenced as 26X8X0X98 cycle paired end reads on an Illumina HiSeq 2500 in rapid mode using TruSeq SBS sequencing kit version 3 and HCS 2.2.58

data collection software. Base-calling was performed using Illumina's RTA version 1.18.64. Fastq files generation from raw sequencing data (BCL files), alignment to the mouse genome reference sequences (build mm10), digital gene expression matrix generation, and conversion to a CSV format were all performed using the 10X Genomics cellranger commands, and data were analyzed using SeqGeq (BDBiosciences).

Supplementary figures

Fig. S1

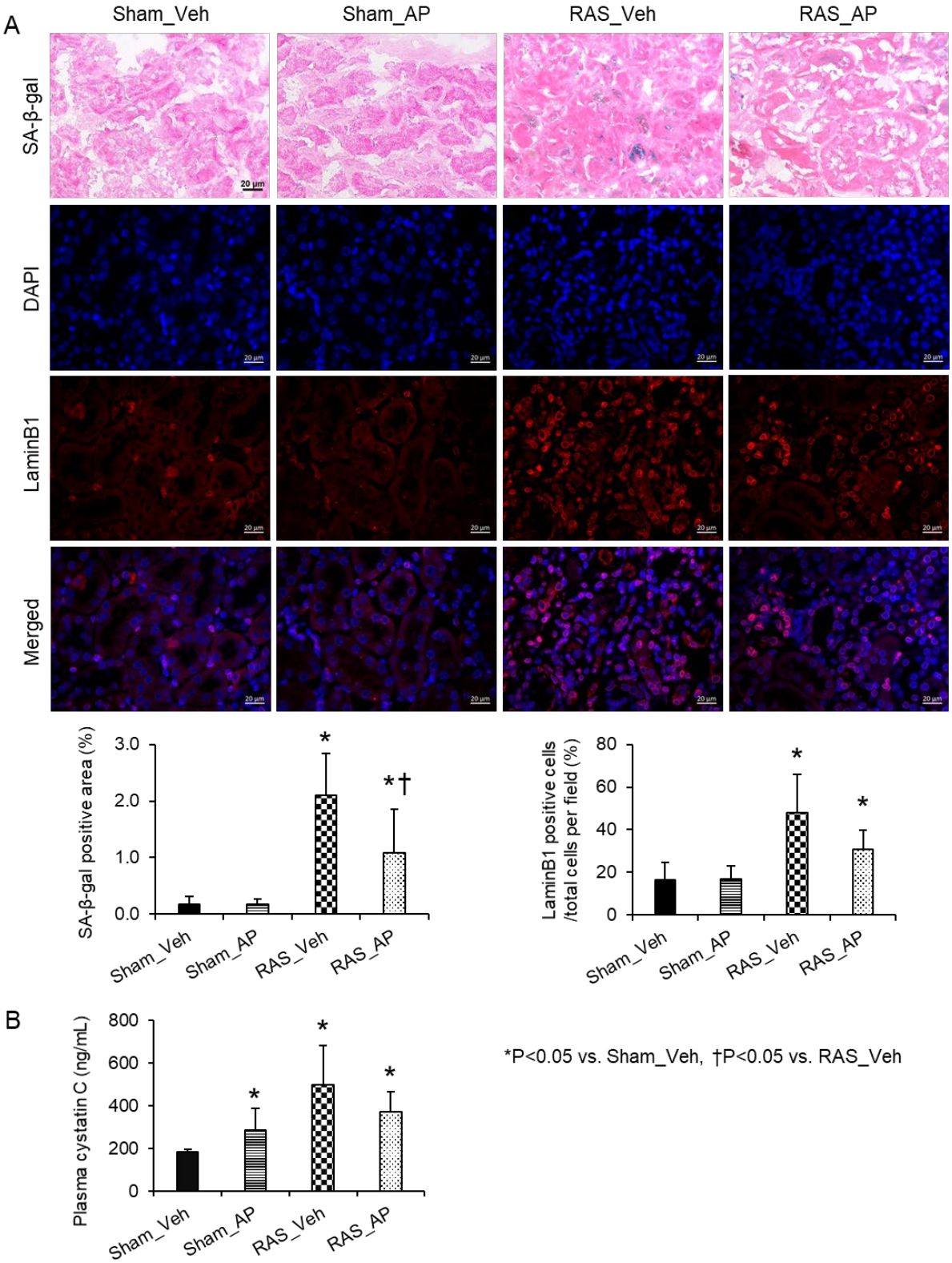

*P<0.05 vs. Sham_Veh, †P<0.05 vs. RAS_Veh

Figure S1. Senescence staining and plasma cystatin C level in 6-week RAS. (A) The percent of SA-β-gal positive area (blue) was increased in the stenotic kidneys, but decreased after AP injection. LaminB1 positive cells (red) out of total cells per field were higher in RAS than in sham, but AP tended to reduce them (p=0.08). blue=DAPI. **(B)** Plasma cystatin C levels were increased in stenotic kidneys compared to Sham_veh, whereas the decrease after AP injection has not reached statistically significant levels *P<0.05 vs. Sham_Veh , †P<0.05 vs. RAS_Veh.

Fig. S2

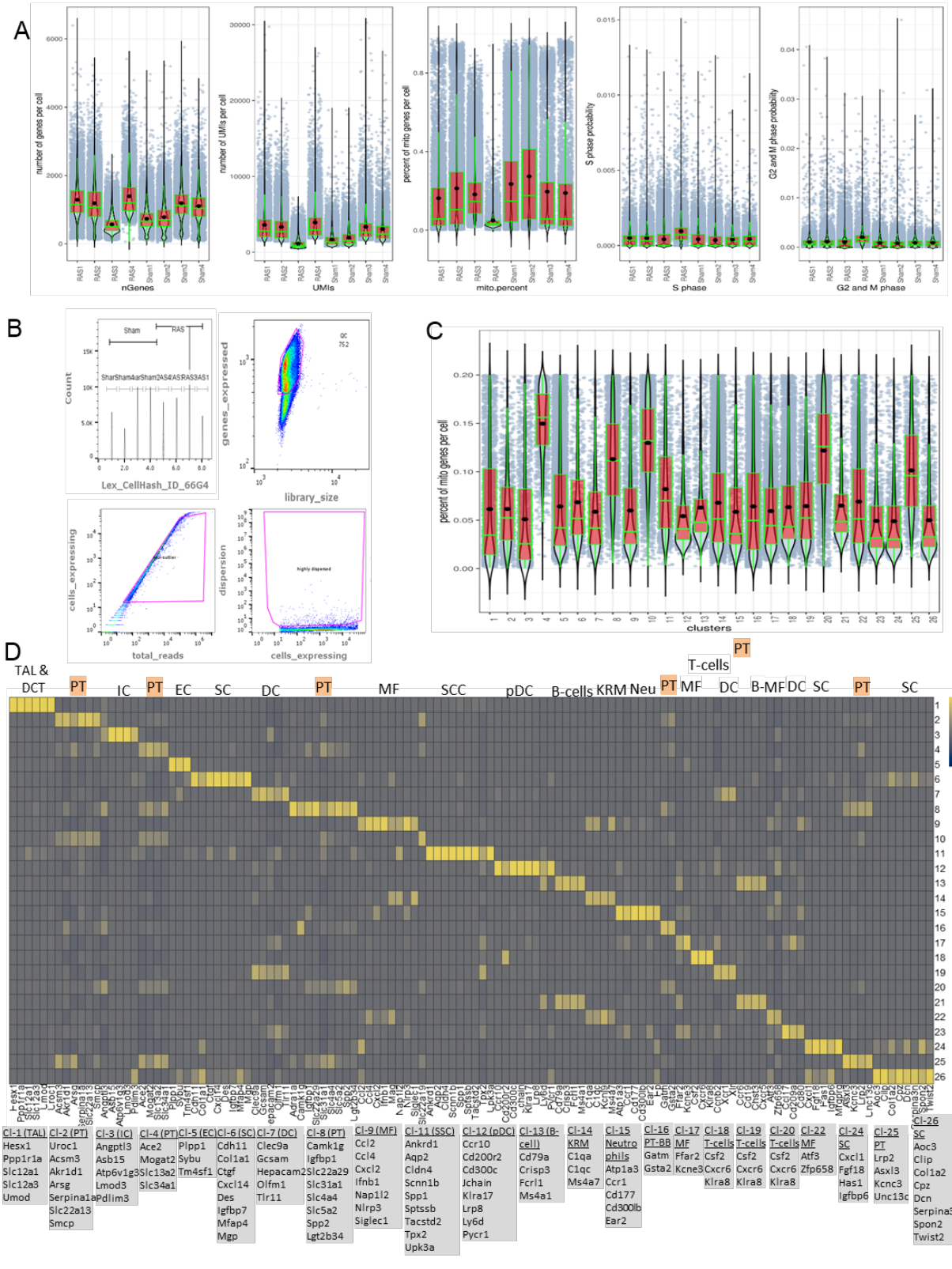
A
number of genes per cell
nGenes
number of UMIs per cell
UMIs
percent of mito genes per cell
mito.percent
S phase probability
S phase
G2 and M phase probability
G2 and M phase
RAS1
RAS2
RAS3
RAS4
Sham1
Sham2
Sham3
Sham4
B
Sham
RAS
Count
Lex_CellHash_ID_66G4
genes_expressed
library_size
cells_expressing
total_reads
dispersion
C
percent of mito genes per cell
clusters
D
TAL & DCT
PT
IC
PT
EC
SC
DC
PT
MF
SCC
pDC
B-cells
KRM
Neu
PT
T-cells
MF
DC
B-MF
DC
SC
PT
SC
Cl-1 (TAL)
Hesx1
Ppp1r1a
Slc12a1
Slc12a3
Umod
Cl-2 (PT)
Uroc1
Acsm3
Akr1d1
Arsg
Serpina1a
Slc22a13
Smcp
Cl-3 (IC)
Angptl3
Asb15
Atp6v1g3
Lmod3
Pdlim3
Cl-4 (PT)
Ace2
Mogat2
Slc13a2
Slc34a1
Cl-5 (EC)
Plpp1
Sybu
Tm4sf1
Cl-6 (SC)
Cdh11
Col1a1
Ctgf
Cxcl14
Des
Igfbp7
Mfap4
Mgp
Cl-7 (DC)
Clec9a
Gcsam
Hepacam2
Olfm1
Tlr11
Cl-8 (PT)
Camk1g
Igfbp1
Slc22a29
Slc31a1
Slc4a4
Slc5a2
Spp2
Lgt2b34
Cl-9 (MF)
Ccl2
Ccl4
Cxcl2
Ifnb1
Nap1l2
Nlrp3
Siglec1
Cl-11 (SSC)
Ankrd1
Aqp2
Cldn4
Scnn1b
Spp1
Sptssb
Tacstd2
Tpx2
Upk3a
Cl-12 (pDC)
Ccr10
Cd200r2
Cd300c
Jchain
Klra17
Lrp8
Ly6d
Pycr1
Cl-13 (B-cell)
Cd79a
Crisp3
Fcrl1
Ms4a1
Cl-14
KRM
C1qa
C1qc
Ms4a7
Cl-15
Neutrophils
Atp1a3
Ccr1
Cd177
Cd300lb
Ear2
Cl-16
PT-BB
Gatm
Gsta2
Cl-17
MF
Ffar2
Kcne3
Cl-18
T-cells
Csf2
Cxcr6
Klra8
Cl-19
T-cells
Csf2
Cxcr6
Klra8
Cl-20
T-cells
Csf2
Cxcr6
Klra8
Cl-22
MF
Atf3
Zfp658
Cl-24
SC
Cxcl1
Fgf18
Has1
Igfbp6
Cl-25
PT
Lrp2
Asxl3
Kcnc3
Unc13c
Cl-26
SC
Aoc3
Clip
Col1a2
Cpz
Dcn
Serpina3n
Spon2
Twist2

Figure S2. Quality Control (QC) of the single-cell RNA (scRNA) sequencing data.

(A), Number of genes per cell, UMIs, mitochondrial percent, S Phase Probability and G2 and M phase probability in individual samples of Sham and RAS. **(B)** QC measures to normalize the scRNA sequencing data in SeqGeq, showing the optimally dispersed gene (ODG) gate used for clustering. Highly expressing mitochondrial genes were removed and the rest used for clustering. Also shown is the number of cells in the 8 sham and RAS samples. **(C),** Distribution of mitochondrial genes in all 26 clusters.

(D) Heatmap showing the mean expression of differentially expressed genes across all the clusters. Clusters with similar lineage as identified by Pseudotime Abstract KNetL maps are highlighted in same colors, Proximal tubules (PT) (light orange), stromal cell clusters. All proximal tubule clusters primarily express *Slc34a1*, *Lrp2,* and Proximal S1 tubule (Cluster8) differentially expressed *Slc5a2* and *Slc4a4*. Four populations of stromal cells were observed. Cluster6 Mgp+ stromal cells differentially expressed *Mgp, Cfh, Igfbp7*. Clusters 24 and 26 Dcn+ stromal cells express *Pi16, Ugdh, Clec3b, Igfbp6*. Profibrotic genes *Col1a1, Col1a2* were expressed by all three stromal cell clusters. Macrophages were identified using typical markers such as *C1qa, C1qb, Ms4a7* etc.

Fig. S3

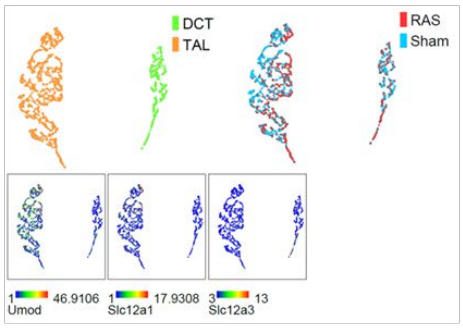
A
DCT
TAL
RAS
Sham
1 46.9106
Umod
1 17.9308
Slc12a1
3 13
Slc12a3

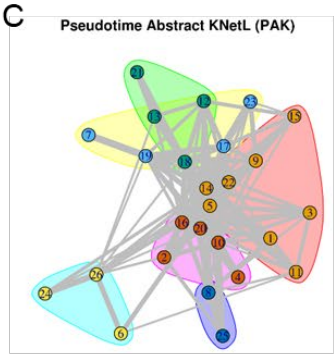
C
Pseudotime Abstract KNetL (PAK)

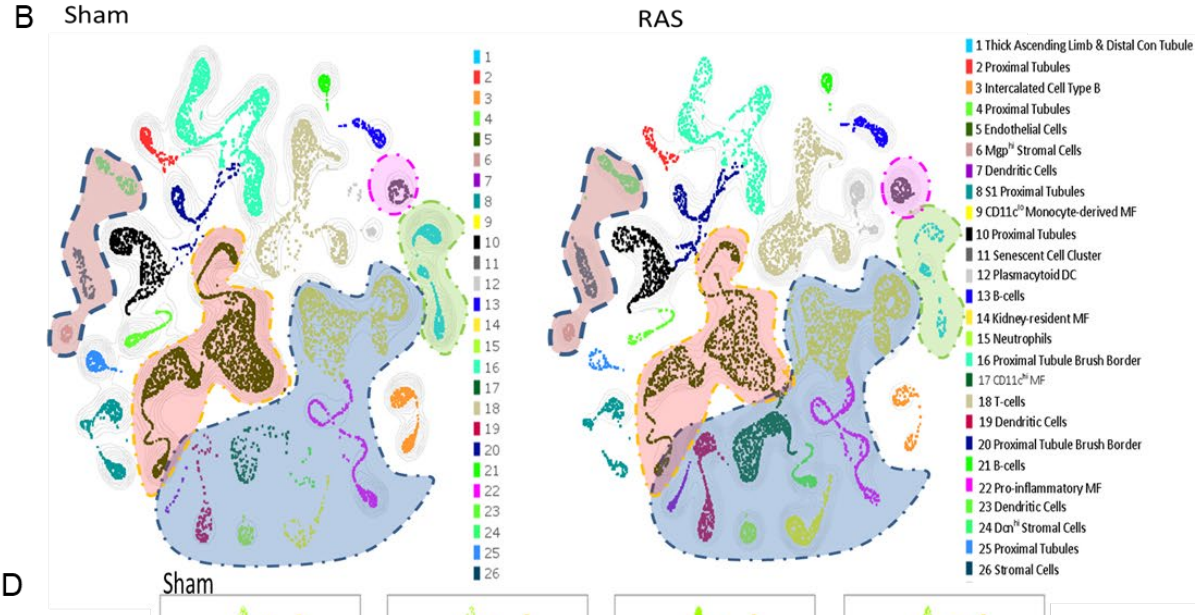
B
Sham
RAS
1 Thick Ascending Limb & Distal Con Tubule
2 Proximal Tubules
3 Intercalated Cell Type B
4 Proximal Tubules
5 Endothelial Cells
6 Mgp^hi Stromal Cells
7 Dendritic Cells
8 S1 Proximal Tubules
9 CD11c^hi Monocyte-derived MF
10 Proximal Tubules
11 Senescent Cell Cluster
12 Plasmacytoid DC
13 B-cells
14 Kidney-resident MF
15 Neutrophils
16 Proximal Tubule Brush Border
17 CD11c^hi MF
18 T-cells
19 Dendritic Cells
20 Proximal Tubule Brush Border
21 B-cells
22 Pro-inflammatory MF
23 Dendritic Cells
24 Dcn^hi Stromal Cells
25 Proximal Tubules
26 Stromal Cells

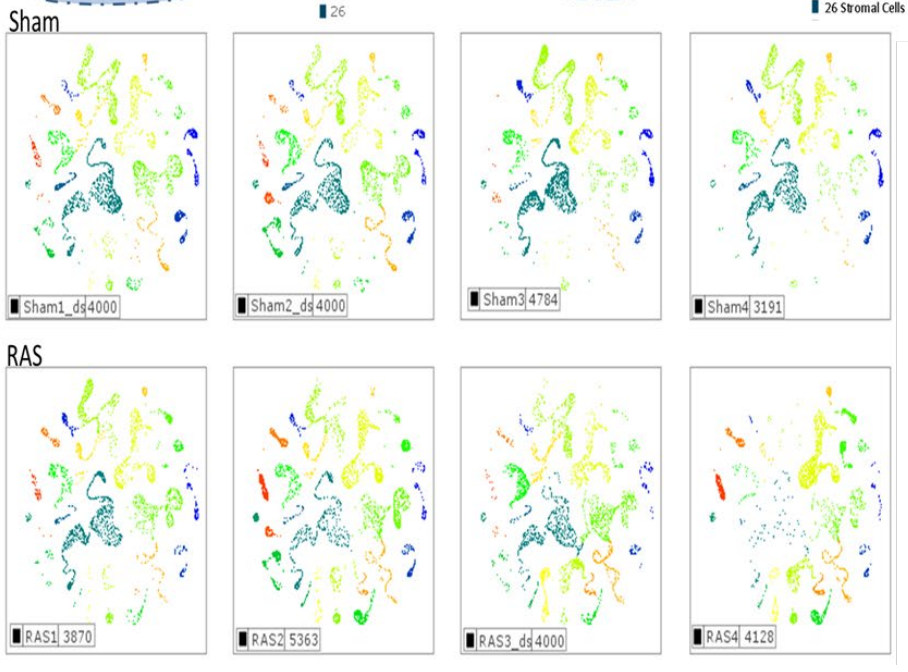
D
Sham
Sham1_ds 4000
Sham2_ds 4000
Sham3 4784
Sham4 3191
RAS
RAS1 3870
RAS2 5363
RAS3_ds 4000
RAS4 4128

Figure S3. Sub-clustering and PAK analysis in Sham and RAS. (A) Sub-clustering to identify Distal Collecting Tubule (DCT) and Thick Ascending Limb Loop of Henle (TAL): Cluster 1 was re-clustered to separate DCT and TAL. DCT differentially express Slc12a3, while TAL expresses Umod and Slc12a1. Because TAL- and DCT-specific genes did not feature among the highly dispersed genes, we did not initially observe independent TAL and DCT clusters. However, upon re-clustering cluster 01, these two populations separated clearly, Both DCT and TAL were reduced in RAS compared to Sham. **(C)** Pseudotime Abstract KNetL maps (PAK maps) generated using iCellR. Each node represents a cluster and the length and thickness of the links (edges) represent distances between each cluster. The shorter and thicker the link, the more closely related (similar) are the cell communities. For example, Clusters 24, 26 and 6 (stromal cells). Similarly, Clusters 3 (Intercalated Cells), 1 (TAL and DCT) and 11 (Senescence Cell Cluster) may be linked. Clusters 7, 19, 17 and 23 are dendritic cells and $CD11c^{hi}$ macrophages. **(B)** KNetL Maps for Sham and RAS Populations: Note the increase of myeloid cell populations (blue), Senescence Cell Cluster (pink), and Stromal Cell Cluster (grey) in RAS compared to Sham. Highlighted are Endothelial cells (orange) and Thick Ascending Limb Loop of Henle Cluster (green) that are reduced in RAS as compared to Sham. **(D)** KNetL Maps for Individual Samples in Sham (top row) and RAS (bottom row) Populations. Note all samples in Sham follow same KNetL fingerprint. In RAS, we observe all the populations that are seen in Sham. However, severity of ischemia has defined cell types. This is evident when comparing RAS1 and RAS4. RAS4 seems to have lost more endothelial cells and has more immune and stromal

cells as compared to RAS1 and 3. Clinical severity defined by reduction in kidney size matches the cell profiles seen above.

Fig. S4

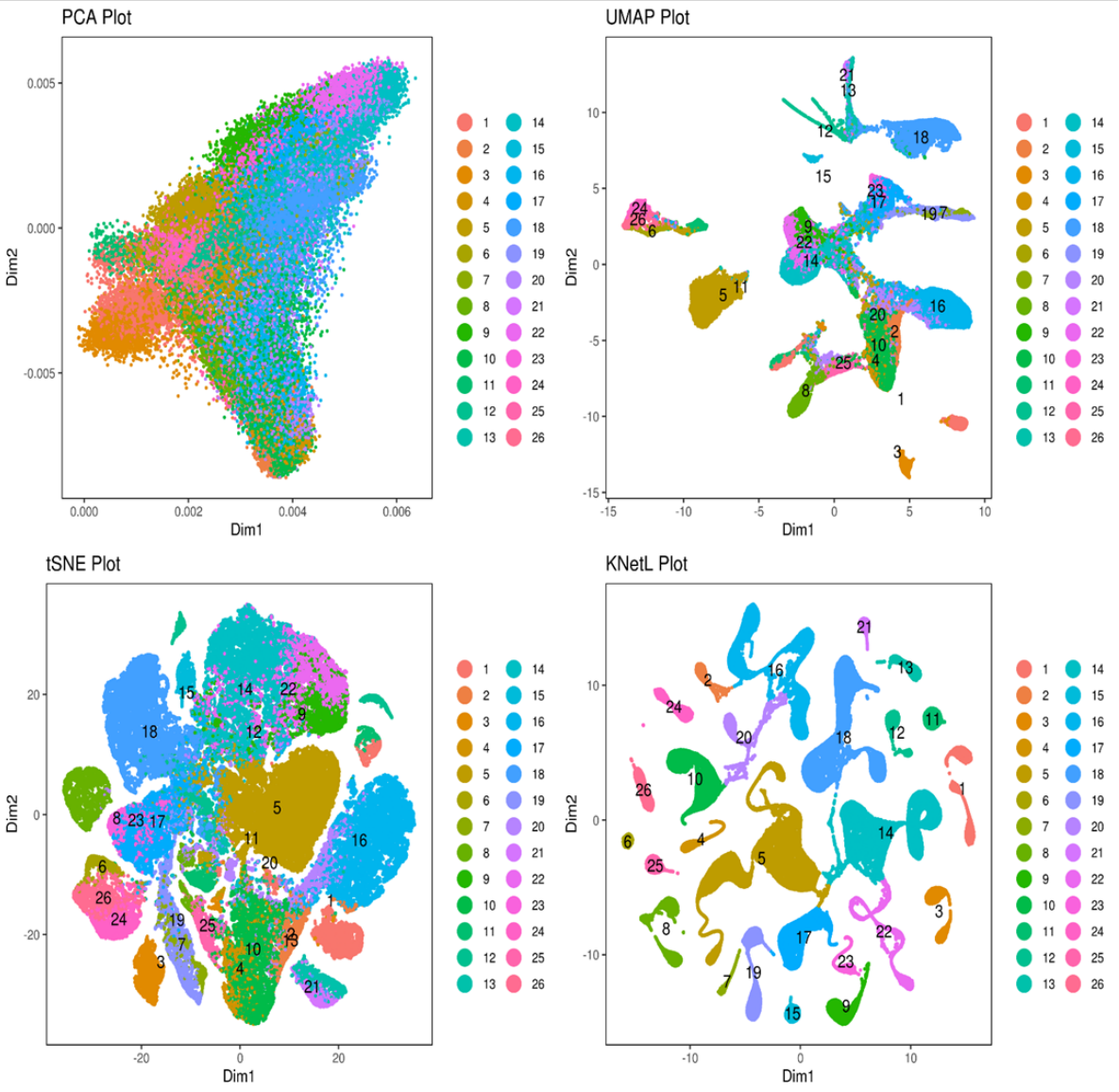

Figure S4. Comparison among tSNE, UMAP and KNetL. Briefly, after quality control the matrix was normalized based on their library sizes. A statistical test was then performed to calculate gene dispersion, base mean and cell coverage to use to build a gene model for performing Principal Component Analysis (PCA) genes with high coverage (top 500) and high dispersion (dispersion > 1.5) were chosen (1413 genes) to perform PCA and batch alignment using iCellR R package (v1.5.5) (https://CRAN.R-

project.org/package=iCellR). T-distributed Stochastic Neighbor Embedding (t-SNE) and Uniform Manifold Approximation and Projection (UMAP) were performed on the top 10 PCs and K-nearest-neighbor-based Network graph drawing Layout (KNetL) was performed based on the top 20 PCs.

Because KNetl has, a significantly higher resolution compared to tSNE and UMAP it is best to use twice more PC dimensions (20 PCs) to avoid plotting many sub-populations (20 PCs often work best for most samples). Additionally, a zoom option in the KNetL map allows adjusting the level of detail (more or fewer sub-populations in cell communities), in here we used a zoom of 600. The network layout used in KNetL map is a force-based layout (Fruchterman and Reingold, 1991) (28) and the zoom option is for changing the force in the system. Force-directed graph drawing algorithms assign attractive (analogous to spring force) and repulsive forces (usually described as analogous to the forces in atomic particles) to separate all pairs of nodes. (Fruchterman and Reingold, 1991) (28). In here, the nodes of the network layout are extracted and UMAP has been performed to create the final plot, a KNetL map. PhenoGraph (Levine et al., Cell, 2015) clustering was then performed on the KNetL map results. Then the marker genes were found for each cluster and visualized on heatmaps, bar plots and box. The marker genes were then used to determine the cell types. Proportion (percentage) of the cell communities in each condition were calculated and Pseudotime Abstract KNetL maps (PAK map) were generated using iCellR. The Tirosh scoring method (Tirosh, et. al. 2016 https://science.sciencemag.org/content/352/6282/189) was used to calculate G0, G1S, G2M, M, G1M and S phase score. The gene lists for G0, G1S, G2M, M, G1M and S phase were chosen from previously published article (Xue,

et.al 2020 https://www.nature.com/articles/s41586-019-1884-x)

Fig. S5

A

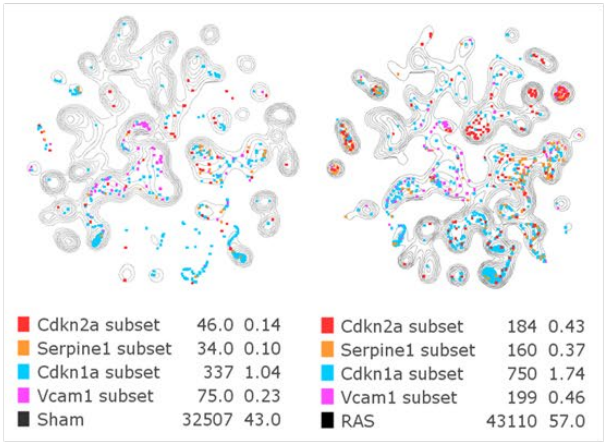

B

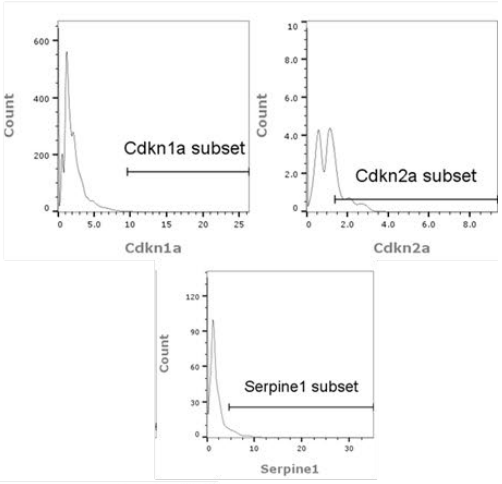

C

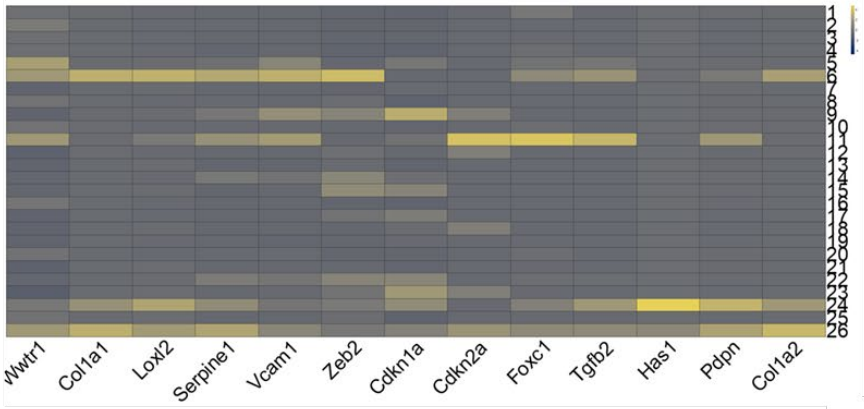

D

Pathways from ~600 genes expressed in Ankrd1+ stromal cells

Term	Overlap	P-value	Adjusted P-value	Odds Ratio	Combined Score
extracellular matrix organization (GO:0030198)	36/229	9.33E-16	4.76E-12	5.062971	175.2208
regulation of cell migration (GO:0030334)	42/316	1.71E-15	4.37E-12	4.28056	145.538
regulated exocytosis (GO:0045055)	28/148	1.26E-14	2.13E-11	6.09305	195.0325
platelet degranulation (GO:0002576)	25/124	7.26E-14	9.26E-11	6.493169	196.4446
positive regulation of cellular process (GO:0048522)	50/519	1.31E-12	1.34E-09	3.102709	84.88369
regulation of cell proliferation (GO:0042127)	61/740	3.69E-12	3.14E-09	2.654829	69.89097
platelet aggregation (GO:0070527)	13/33	7.13E-12	5.20E-09	12.68726	325.6402
positive regulation of cell differentiation (GO:0045597)	28/194	1.27E-11	8.10E-09	4.648306	116.6215
homotypic cell-cell adhesion (GO:0034109)	13/38	5.84E-11	3.31E-08	11.01788	259.6236
regulation of apoptotic process (GO:0042981)	62/815	7.05E-11	3.60E-08	2.450036	57.2691
cell junction assembly (GO:0034329)	15/59	2.29E-10	1.06E-07	8.187996	181.752
muscle contraction (GO:0006936)	22/137	2.50E-10	1.06E-07	5.171786	114.3469
positive regulation of transcription from RNA polymerase II promoter (GO:0045944)	61/848	9.28E-10	3.64E-07	2.316714	48.18226
regulation of transcription from RNA polymerase II promoter (GO:0006357)	88/1478	2.32E-09	8.47E-07	1.91755	38.12183
positive regulation of cell proliferation (GO:0008284)	37/424	1.73E-08	5.88E-06	2.81044	50.23327
positive regulation of transcription, DNA-templated (GO:0045893)	70/1120	1.84E-08	5.86E-06	2.012882	35.85572
cellular protein metabolic process (GO:0044267)	40/484	2.07E-08	6.21E-06	2.661663	47.09527
positive regulation of cellular biosynthetic process (GO:0031328)	21/159	2.34E-08	6.64E-06	4.253638	74.73376
positive regulation of cell migration (GO:0030335)	25/221	2.66E-08	7.14E-06	3.643226	63.54719
negative regulation of cell migration (GO:0030336)	18/121	3.66E-08	9.35E-06	4.790993	82.03342
regulation of cell differentiation (GO:0045595)	18/121	3.66E-08	8.90E-06	4.790993	82.03342
regulation of cell death (GO:0010941)	16/96	4.08E-08	9.45E-06	5.367687	91.33533
regulation of transmembrane receptor protein serine/threonine kinase signaling pathway (GO:0090092)	28-Sep	1.03E-07	2.29E-05	10.35197	166.5381
regulation of epithelial to mesenchymal transition (GO:0010717)	13/68	1.44E-07	3.06E-05	6.157052	97.00418
negative regulation of cell motility (GO:2000146)	15/97	2.99E-07	6.09E-05	4.980328	74.82579
negative regulation of transcription, DNA-templated (GO:0045892)	53/813	3.04E-07	5.97E-05	2.099538	31.50458
positive regulation of apoptotic process (GO:0043065)	28/307	3.93E-07	7.44E-05	2.937366	43.32137
positive regulation of macromolecule biosynthetic process (GO:0010557)	18/142	4.38E-07	7.98E-05	4.082466	59.77469
cellular response to transforming growth factor beta stimulus (GO:0071560)	15/100	4.49E-07	7.89E-05	4.830918	70.61456

E

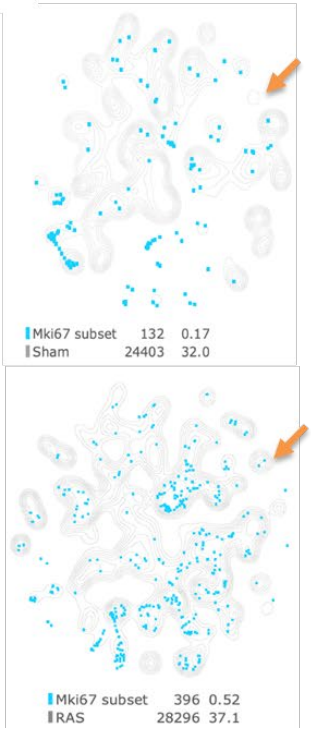

Figure S5. Mapping Senescent cell clusters in Sham and RAS. (A) Overlay of Cdkn2a, Cdkn1a, and Serpine1 (as well as Vcam1) on Sham and RAS to identify senescent cell clusters. Native clusters in Sham and RAS are presented as contours for better identification. RAS has ~4-fold higher Cdkn2a^{+} (184 vs 46) and Serpine^{+} (160 vs 34) cells, and 2-fold higher Vcam1^{+} cells than Sham. Clusters 11 and 26 expressed Cdkn1a, Serpine1, and Cdkn2a. **(B)** Gates set to include Cdkn2a, Cdkn1a and Serpine1 cells. **(C)** Heatmap shows mean expression of Serpine1, Cdkn1a, Cdkn2a and genes regulating epithelial to mesenchymal transition in individual clusters (Y-axis). Note Clusters 11 and 26 both express all three genes, but Vcam1 was differentially expressed in cluster 11. Therefore, we chose to further investigate cluster 11. **(D)** Pathway analysis (using Enrichr) of Ankrd1+ Stromal cells showing about 600 differentially expressed genes. The pathway analysis predicts that Ankrd1+ stromal cells may be in early phases of epithelial to mesenchymal transition (GO:0010717). **(E)** *Mki67*+ cells in Sham and RAS. Note, Cluster 11 (orange arrows) shows very few Mki67+ cells.

Fig. S6

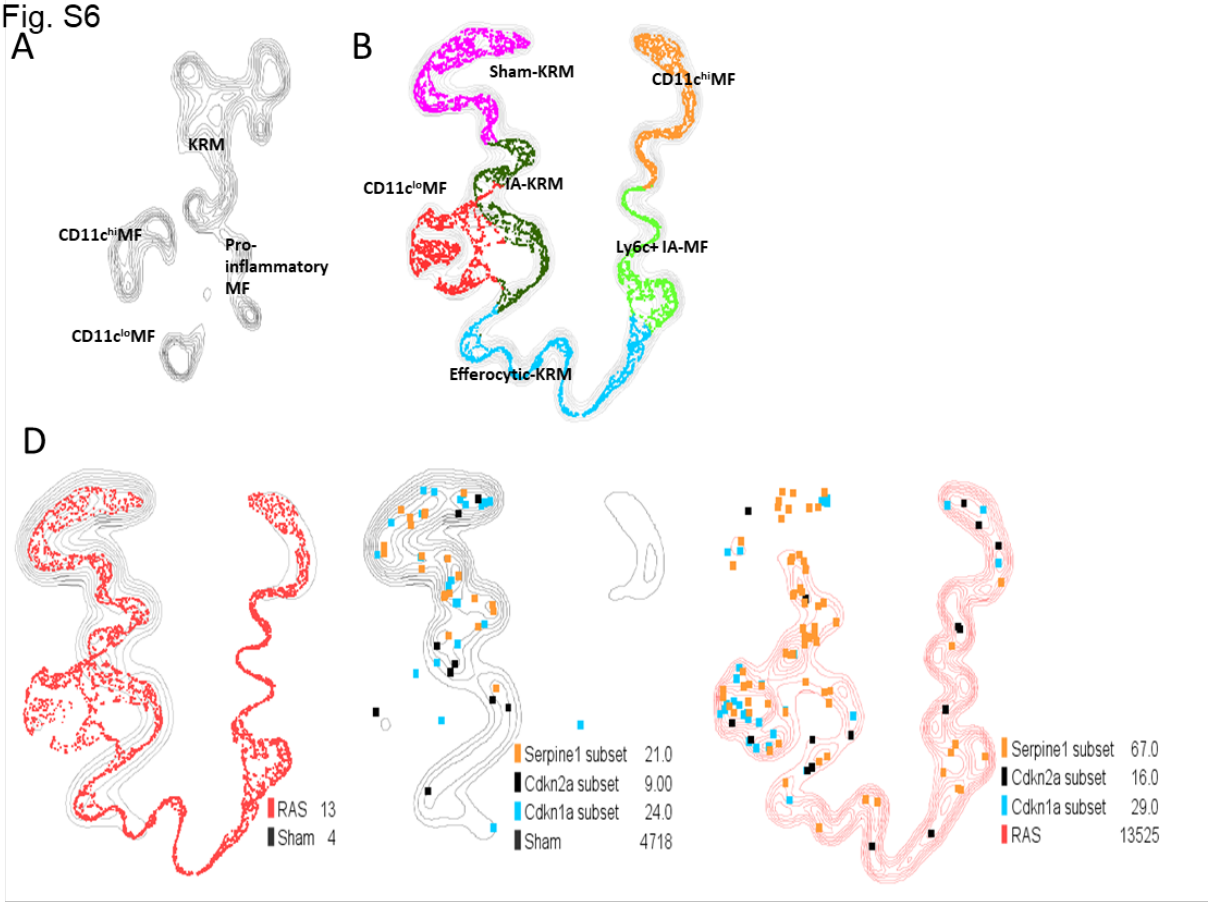
A
KRM
CD11c^hiMF
Pro-inflammatory MF
CD11c^loMF
B
Sham-KRM
CD11c^hiMF
CD11c^loMF
IA-KRM
Ly6c+ IA-MF
Efferocytic-KRM
D
RAS 13
Sham 4
Serpine1 subset 21.0
Cdkn2a subset 9.00
Cdkn1a subset 24.0
Sham 4718
Serpine1 subset 67.0
Cdkn2a subset 16.0
Cdkn1a subset 29.0
RAS 13525

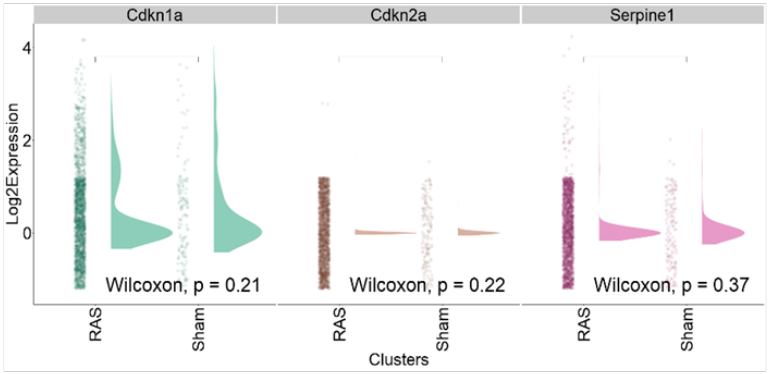
C
Cdkn1a
Cdkn2a
Serpine1
Log2Expression
4
2
0
Wilcoxon, p = 0.21
Wilcoxon, p = 0.22
Wilcoxon, p = 0.37
RAS
Sham
Clusters

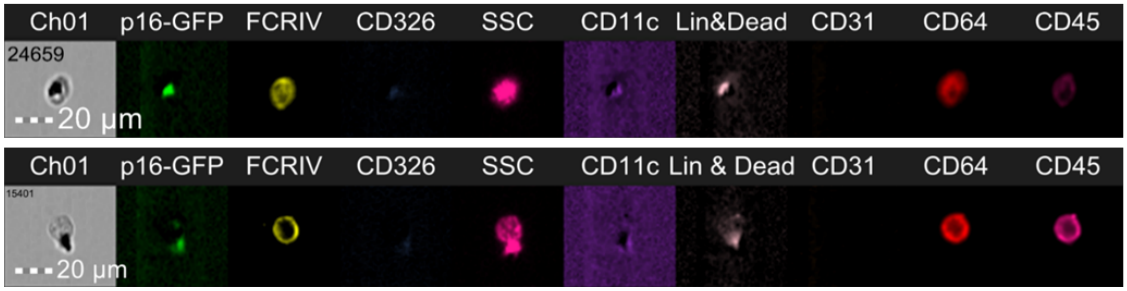
E
Ch01 p16-GFP FCRIV CD326 SSC CD11c Lin&Dead CD31 CD64 CD45
24659
20 µm
Ch01 p16-GFP FCRIV CD326 SSC CD11c Lin & Dead CD31 CD64 CD45
15401
20 µm

Figure S6. Macrophages expressing senescent genes significantly increase in RAS. (A) We probed kidney-resident macrophages, CD11c^{hi} and CD11c^{lo} macrophage clusters, and proinflammatory macrophages to see which macrophages underwent senescence. **(B)** Re-clustering all macrophages identified a population of ischemia-associated KRM (IA-KRM) unique to RAS-kidneys. We also observed CD11c^{hi} and CD11c^{lo} macrophages and a small population of efferocytic macrophages. **(C)** Macrophages do not upregulate the expression of senescent genes in RAS-kidneys. **(D)** However, macrophage numbers increase in RAS. Number of macrophages expressing senescent genes also increase in RAS as compared to Sham. Most senescent genes cluster in CD11c^{lo} macrophages that are predominantly pro-inflammatory. This suggest that infiltrating monocyte-derived macrophages may express senescent genes as compared to the kidney-resident macrophages **(E)** To further probe if macrophages undergo senescence, we used the p16^{INKATTAC} mice to observe that majority of FCRIV+CD64+ macrophages rather than expressing p16-GFP have engulfed the GFP+ particles suggesting that macrophages efferocytose senescent cells.

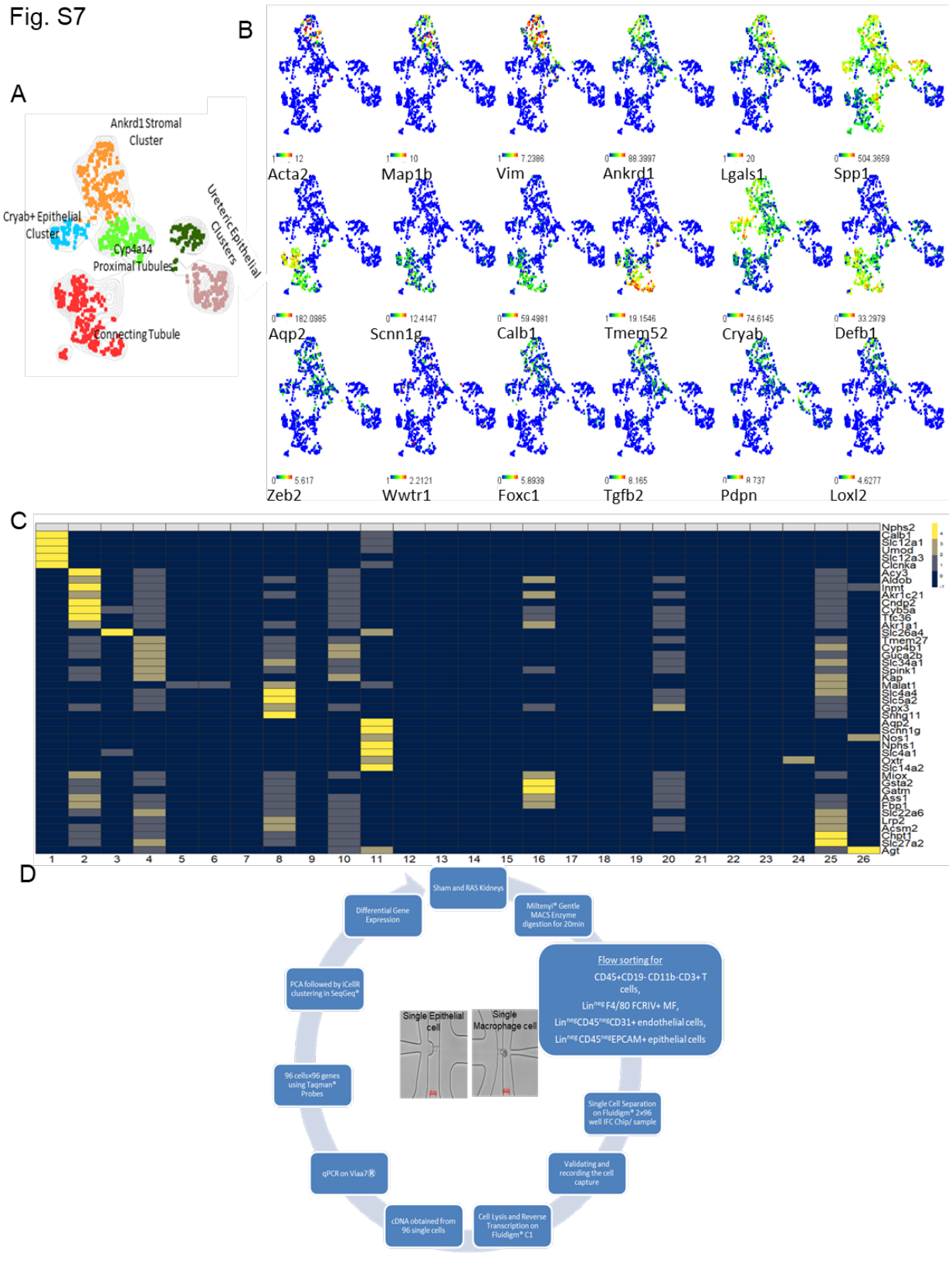

Figure S7. UMAP plots representing genes preferentially expressed in Ankrd1+

Stromal Cell Cluster. (A) Re-clustering cluster 11 separated 5 clusters**. (B)** Connecting tubules express Aqp2, Scnn1g Calb1 and Tmem52b (row 2). Ankrd1+ stromal cells express epithelial genes such as Spp1, Cryab (row 1) and mesenchymal genes such as Vim, Map1b, Lgals1, Tsc22d1, (row 1). Ankrd1+ Stromal cells differentially upregulated transcription factor such as Zeb2, Tgfb2 and genes such as Wwtr1, Foxc1, Pdpn and Loxl2 suggesting that these cells are undergoing epithelial-to-mesenchymal (EMT) transition (last row). **(C)** Heatmap showing differentially expressed tubular markers (y-axis) in all the clusters (x-axis). Note cluster 11 differentially express many tubular markers such as Aqp2, Slc4a1, Scnn1g etc. **(D)** Single-cell qPCR workflow: Experimental design for isolating viable epithelial cells (epi), endothelial cells, macrophages (MF) and T-cells from Sham and RAS kidneys. Kidneys were digested and flow sorted. ~192 single cells (~48 per population) underwent QPCR for 96 genes. Representative cell image of macrophage and epithelial cell shown as captured on Apotome at 10X and 40X.

Fig. S8

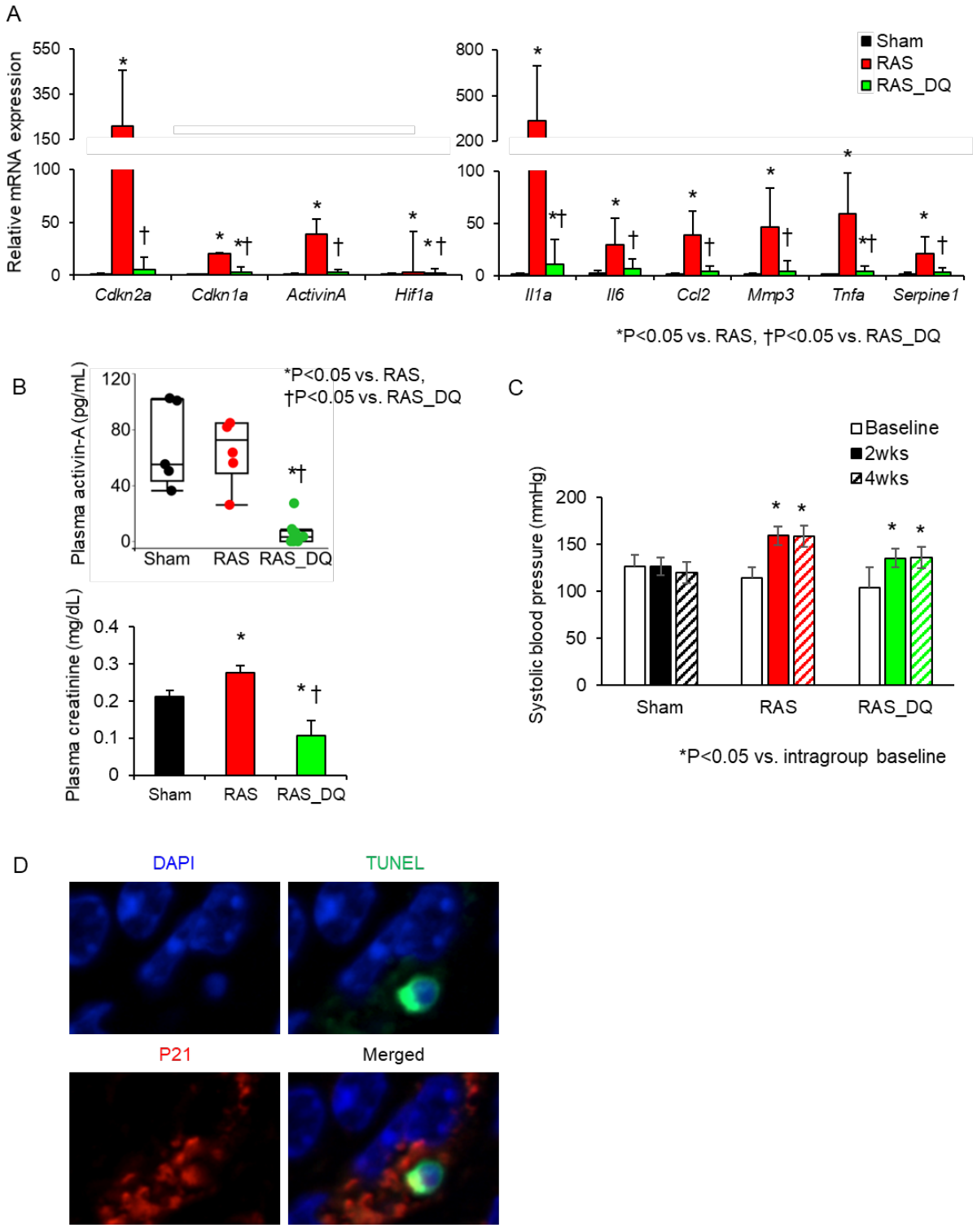

Figure S8. DQ alleviates stenotic kidney cellular senescence in RAS. (A) Renal gene expression of senescence and SASP factors (relative to GAPDH). **(B)** Plasma

levels of Activin-A and creatinine. *P<0.05 vs. RAS, †P<0.05 vs. RAS_DQ. **(C)** Systolic blood pressures at 0, 2, and 4 weeks. *P<0.05 vs. intragroup baseline. **(D)** Double-staining with p21 and TUNEL on STK sections of DQ-treated mice.

Fig. S9

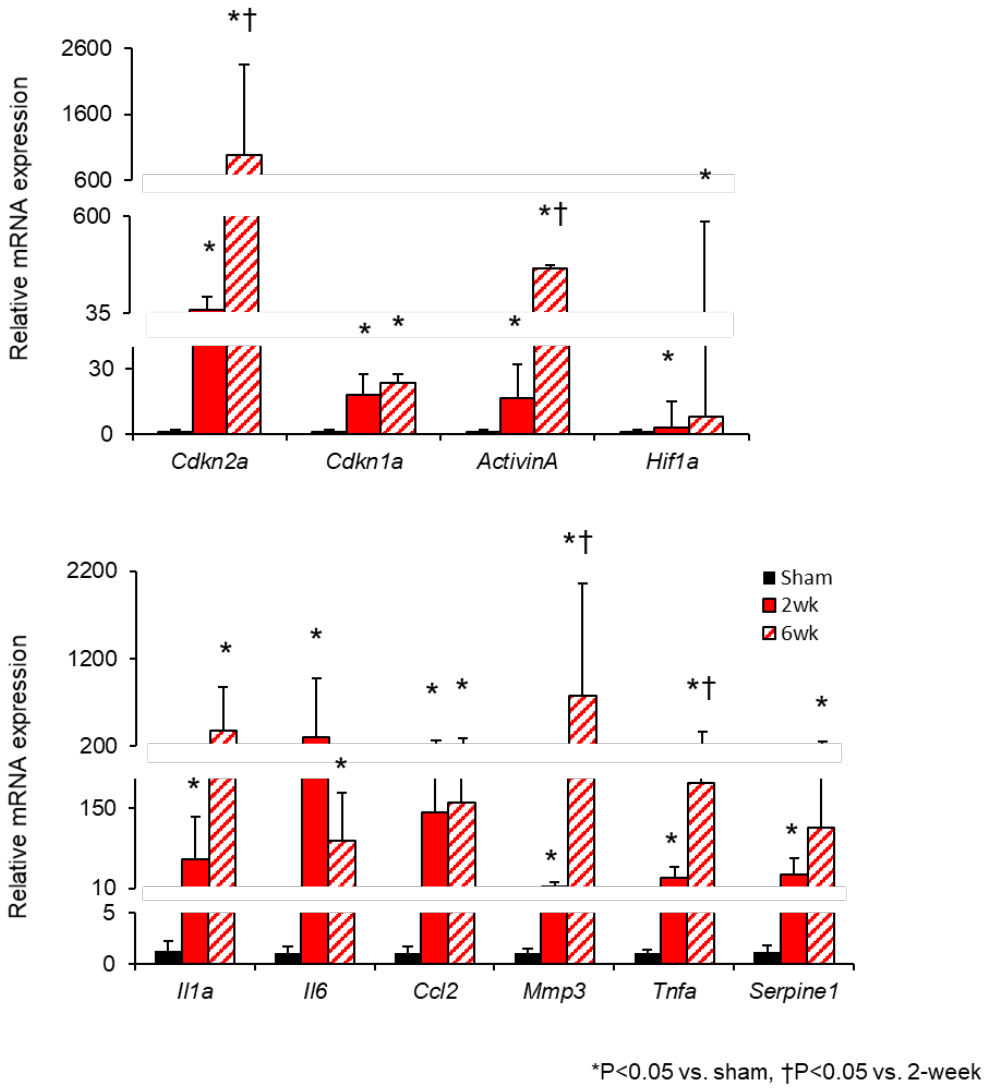

Figure S9. Renal gene expression of senescence and SASP factors in sham, 2-week RAS, and 6-week RAS, quantified by RT-PCR relative to GAPDH.

Fig. S10

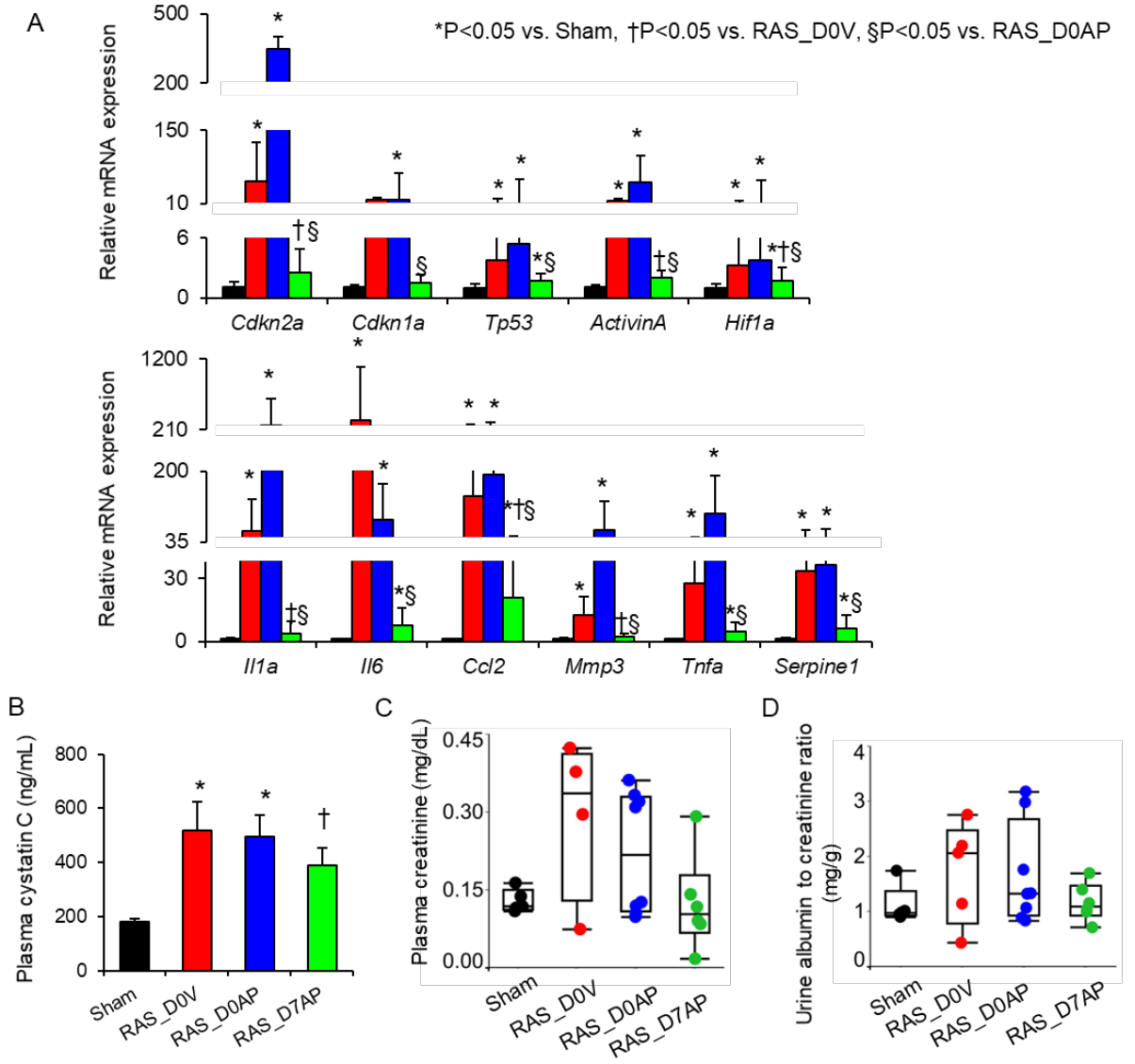

*P<0.05 vs. Sham, †P<0.05 vs. RAS_D0AP

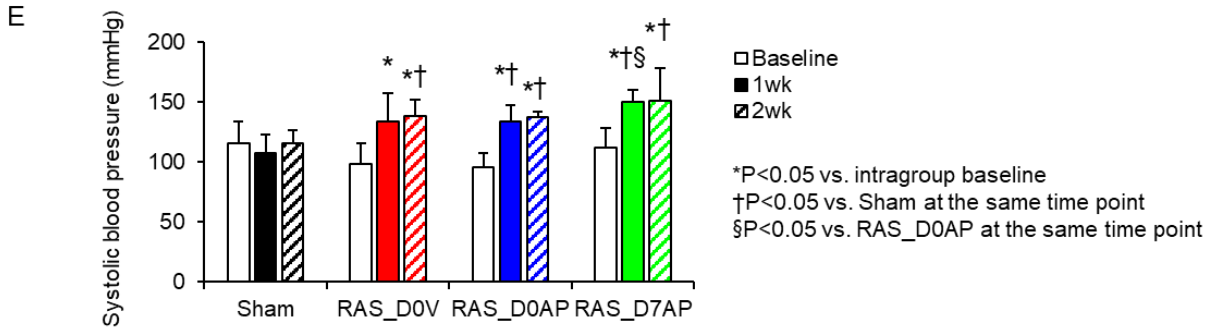

Figure S10. Senescence in STK is initially protective but ultimately drives persistent injury. (A) Renal gene expression of senescence and SASP factors quantified by RT-PCR relative to GAPDH levels decreased after AP delivery starting at D7, but not at D0. **(B)-(D)** Plasma cystatin C, creatinine levels, and urine albumin/creatinine ratio. *P<0.05 vs. Sham, †P<0.05 vs. RAS_D0AP. E, Systolic blood pressures at 0, 1, and 2 weeks. *P<0.05 *vs*. intragroup baseline. †P<0.05 vs. Sham at the same time point, §P<0.05 vs. RAS_D0AP at the same time point.

Supplementary table: Characteristics of mice

		Body weight (g)		Kidney weight (mg)	
Model	Group	Basal	Final	Right/stenotic	Left/contralateral
INK-ATTAC transgenic mice 6 weeks after sham or RAS surgeries, with or without AP20187(AP) treatment started 2 weeks later	Sham_Veh	25.9±1.7	26.7±3.2	221.8±51.4	213.7±40.6
	Sham_AP	31.3±3.5*	31.2±3.9*	231.8±37.0	217.8±35.2
	RAS_Veh	29.4±3.5*	27.7±2.8†	68.9±13.1*†$	264.9±68.8
	RAS_AP	25.3±3.9†§	23.3±1.6†§	80.3±36.1*†$	199.1±34.0
C57/BL6 mice treated with DQ starting two weeks after RAS surgery	Sham	31.2±1.3	30.9±1.6	225.0±29.9	214.0±14.5
	RAS	31.1±2.3	28.0±1.4*	72.2±32.3*	229.0±24.7
	RAS_DQ	33.1±2.7	28.2±1.6*	172.9±28.3*†	212.6±25.2
INK-ATTAC transgenic mice 2 weeks after sham or RAS, with AP or vehicle started either immediately (RAS_D0V, RAS-D0AP) or 7 days (RAS-D7AP) after RAS	Sham	26.7±0.7	26.9±2.0	228.0±26.3	235.2±26.6
	RAS_D0V	28.6±3.0	27.4±4.3	132±77.7*	237.0±35.6
	RAS_D0AP	30.3±2.5*	27.1±1.5	104.6±39.1*	252.3±34.2
	RAS_D7AP	26.5±1.5§	26.3±1.7	170.3±28.6*§	231.8±24.8

All Data are mean±SD.

INK-ATTAC transgenic mice 6 weeks after sham or RAS surgeries. *P<0.05 *vs*. Sham_Veh, †P<0.05 vs. Sham_AP, §P<0.05 *vs*. RAS_Veh, $ p<0.05 *vs*. contralateral kidney

C57/BL6 mice treated with DQ. *P<0.05 *vs*. Sham, †P<0.05 *vs*. RAS

INK-ATTAC transgenic mice with RAS studied for 2 weeks. *P<0.05 *vs*. Sham, †P<0.05 *vs*. RAS_D0V, §P<0.05 *vs*. RAS_D0AP

Supplementary data file

Data file S1. Cluster-specific marker genes

Data file S2. Immgen-based cell call

References

1. Baker DJ, Wijshake T, Tchkonia T, LeBrasseur NK, Childs BG, van de Sluis B, et al.: Clearance of p16Ink4a-positive senescent cells delays ageing-associated disorders. *Nature,* 479**:** 232-236, 2011 10.1038/nature10600
2. Jiang K, Ponzo TA, Tang H, Mishra PK, Macura SI, Lerman LO: Multiparametric MRI detects longitudinal evolution of folic acid-induced nephropathy in mice. *Am J Physiol Renal Physiol,* 315**:** F1252-F1260, 2018 10.1152/ajprenal.00128.2018
3. Hall BM, Balan V, Gleiberman AS, Strom E, Krasnov P, Virtuoso LP, et al.: p16(Ink4a) and senescence-associated beta-galactosidase can be induced in macrophages as part of a reversible response to physiological stimuli. *Aging (Albany NY),* 9**:** 1867-1884, 2017 10.18632/aging.101268
4. Xu M, Pirtskhalava T, Farr JN, Weigand BM, Palmer AK, Weivoda MM, et al.: Senolytics improve physical function and increase lifespan in old age. *Nat Med,* 24**:** 1246-1256, 2018 10.1038/s41591-018-0092-9
5. Schafer MJ, White TA, Iijima K, Haak AJ, Ligresti G, Atkinson EJ, et al.: Cellular senescence mediates fibrotic pulmonary disease. *Nat Commun,* 8**:** 14532, 2017 10.1038/ncomms14532
6. Ebrahimi B, Crane JA, Knudsen BE, Macura SI, Grande JP, Lerman LO: Evolution of cardiac and renal impairment detected by high-field cardiovascular magnetic

resonance in mice with renal artery stenosis. *J Cardiovasc Magn Reson,* 15**:** 98, 2013 10.1186/1532-429X-15-98

7. Levine JH, Simonds EF, Bendall SC, Davis KL, Amir el AD, Tadmor MD, et al.: Data-Driven Phenotypic Dissection of AML Reveals Progenitor-like Cells that Correlate with Prognosis. *Cell,* 162**:** 184-197, 2015 10.1016/j.cell.2015.05.047
8. Han X, Wang R, Zhou Y, Fei L, Sun H, Lai S, et al.: Mapping the Mouse Cell Atlas by Microwell-Seq. *Cell,* 173**:** 1307, 2018 10.1016/j.cell.2018.05.012
9. Tabula Muris C, Overall c, Logistical c, Organ c, processing, Library p, et al.: Single-cell transcriptomics of 20 mouse organs creates a Tabula Muris. *Nature,* 562**:** 367-372, 2018 10.1038/s41586-018-0590-4
10. Schaum N, Lehallier B, Hahn O, Palovics R, Hosseinzadeh S, Lee SE, et al.: Ageing hallmarks exhibit organ-specific temporal signatures. *Nature,* 583**:** 596-602, 2020 10.1038/s41586-020-2499-y
11. Tabula Muris C: A single-cell transcriptomic atlas characterizes ageing tissues in the mouse. *Nature,* 583**:** 590-595, 2020 10.1038/s41586-020-2496-1
12. Heng TS, Painter MW, Immunological Genome Project C: The Immunological Genome Project: networks of gene expression in immune cells. *Nat Immunol,* 9**:** 1091-1094, 2008 10.1038/ni1008-1091
13. Puranik AS, Leaf IA, Jensen MA, Hedayat AF, Saad A, Kim KW, et al.: Kidney-resident macrophages promote a proangiogenic environment in the normal and chronically ischemic mouse kidney. *Sci Rep,* 8**:** 13948, 2018 10.1038/s41598-018-31887-4

14. Chen L, Lee JW, Chou CL, Nair AV, Battistone MA, Paunescu TG, et al.: Transcriptomes of major renal collecting duct cell types in mouse identified by single-cell RNA-seq. *Proc Natl Acad Sci U S A,* 114**:** E9989-E9998, 2017 10.1073/pnas.1710964114

15. Jiang K, Ferguson CM, Ebrahimi B, Tang H, Kline TL, Burningham TA, et al.: Noninvasive Assessment of Renal Fibrosis with Magnetization Transfer MR Imaging: Validation and Evaluation in Murine Renal Artery Stenosis. *Radiology,* 283**:** 77-86, 2017 10.1148/radiol.2016160566

16. Cheng J, Zhou W, Warner GM, Knudsen BE, Garovic VD, Gray CE, et al.: Temporal analysis of signaling pathways activated in a murine model of two-kidney, one-clip hypertension. *Am J Physiol Renal Physiol,* 297**:** F1055-1068, 2009 10.1152/ajprenal.90439.2008

17. Livak KJ, Schmittgen TD: Analysis of relative gene expression data using real-time quantitative PCR and the 2(-Delta Delta C(T)) Method. *Methods,* 25**:** 402-408, 2001 10.1006/meth.2001.1262

18. Debacq-Chainiaux F, Erusalimsky JD, Campisi J, Toussaint O: Protocols to detect senescence-associated beta-galactosidase (SA-betagal) activity, a biomarker of senescent cells in culture and in vivo. *Nat Protoc,* 4**:** 1798-1806, 2009 10.1038/nprot.2009.191

19. Melk A, Kittikowit W, Sandhu I, Halloran KM, Grimm P, Schmidt BM, et al.: Cell senescence in rat kidneys in vivo increases with growth and age despite lack of telomere shortening. *Kidney Int,* 63**:** 2134-2143, 2003 10.1046/j.1523-1755.2003.00032.x

20. Ma L, Liu Y, Landry NK, El-Achkar TM, Lieske JC, Wu XR: Point mutation in D8C domain of Tamm-Horsfall protein/uromodulin in transgenic mice causes progressive renal damage and hyperuricemia. *PLoS One,* 12**:** e0186769, 2017 10.1371/journal.pone.0186769

21. Sharif R, Fowler B, Karamichos D: Collagen cross-linking impact on keratoconus extracellular matrix. *PLoS One,* 13**:** e0200704, 2018 10.1371/journal.pone.0200704

22. Korsmo MJ, Ebrahimi B, Eirin A, Woollard JR, Krier JD, Crane JA, et al.: Magnetic resonance elastography noninvasively detects in vivo renal medullary fibrosis secondary to swine renal artery stenosis. *Invest Radiol,* 48**:** 61-68, 2013 10.1097/RLI.0b013e31827a4990

23. Zhang X, Krier JD, Amador Carrascal C, Greenleaf JF, Ebrahimi B, Hedayat AF, et al.: Low-Energy Shockwave Therapy Improves Ischemic Kidney Microcirculation. *J Am Soc Nephrol,* 27**:** 3715-3724, 2016 10.1681/ASN.2015060704

24. Hou J, Cai S, Kitajima Y, Fujino M, Ito H, Takahashi K, et al.: 5-Aminolevulinic acid combined with ferrous iron induces carbon monoxide generation in mouse kidneys and protects from renal ischemia-reperfusion injury. *Am J Physiol Renal Physiol,* 305**:** F1149-1157, 2013 10.1152/ajprenal.00275.2013

25. Kuleshov MV, Jones MR, Rouillard AD, Fernandez NF, Duan Q, Wang Z, et al.: Enrichr: a comprehensive gene set enrichment analysis web server 2016 update. *Nucleic Acids Res,* 44**:** W90-97, 2016 10.1093/nar/gkw377